processes

MDPI

Article

Leakage Dispersion Characteristics and High-Concentration Risk Zoning of Liquid CO_2 Storage Tanks in Oilfield CCUS System Based on a PHAST-KFX Two-Stage Simulation Framework

Weichao Duan [1,2], Jingjing Mu [1,2], Anna Zhou [1,2], Xiaoyu Wang [3], Yue Qi [3], Yanbin Bi [3] and Dongfeng Zhao [2,4,*]

1. Qingdao Oasis SafeViron Tech Co., Ltd., Qingdao 266520, China; dwc@upchse.com (W.D.); mjj@upchse.com (J.M.); zhouan@upchse.com (A.Z.)
2. Safety, Environmental Protection and Energy Conservation Technology Center, China University of Petroleum (East China), Qingdao 266580, China
3. Safety and Environmental Protection Technology Supervision Center, PetroChina Liaohe Oilfield Company, Panjin 124010, China; w_xiaoyu@petrochina.com.cn (X.W.); qiyue2022@petrochina.com.cn (Y.Q.); biyb@petrochina.com.cn (Y.B.)
4. College of Chemical Engineering, China University of Petroleum (East China), Qingdao 266580, China

* Correspondence: 20240022@upc.edu.cn

Abstract

The leakage and dispersion behavior of CO_2 in the ground injection stage of oilfield CCUS systems is highly complex under high-pressure, low-temperature, and continuous-operation conditions, while quantitative criteria for emergency control distances remain insufficient. To address this issue, a liquid CO_2 storage tank in an oilfield CO_2 cyclic injection station was selected as the research object. A 1:1 two-dimensional and three-dimensional computational model was established. A two-stage simulation framework was developed in this study, where PHAST was first employed for rapid multi-scenario consequence screening, followed by three-dimensional CFD validation using KFX under representative high-risk scenarios. The proposed framework was used to systematically investigate CO_2 leakage and dispersion characteristics under various leakage aperture sizes, ambient temperatures, and wind speed conditions. Risk zoning and risk quantification were further conducted based on high-concentration CO_2 toxicity thresholds of 10%, 15%, 20%, and 30%. The results show that the leak aperture is the dominant factor controlling dispersion consequences. As the aperture increased from 5 mm to 50 mm, the maximum dispersion distance increased from 8.8–9.4 m to 132–146 m, and the maximum cloud footprint increased from 4.8–5.4 m^2 to 2204.1–2599.6 m^2. Higher temperature enhanced CO_2 dispersion capacity, whereas wind speed exerted a dual effect involving near-field dilution and downwind transport. The KFX three-dimensional simulation indicated that buildings and equipment arrangements induced near-ground flow separation and local accumulation. Under a 25 mm leak and an average wind speed of 4.6 $m \cdot s^{-1}$, the cloud approached full coverage of the injection station within approximately 300 s and tended to spread beyond the site boundary. Liquid CO_2 leakage was accompanied by flashing, dry-ice formation, and sublimation, leading to a leakage-rate pattern characterized by an initial decrease followed by an increase and gradual stabilization. This indicates that emergency response should account for the ice-plugging and de-plugging process. The risk zoning results show that the downwind region can be divided into fatal, severe-injury, minor-injury, adverse-reaction, and relatively safe zones. A risk level on the order of 10^{-6} still existed at 100 m from the leakage source. It is recommended that CO_2 concentration monitoring and alarm systems be deployed within 100 m of the station, warning signs be placed near the maximum impact boundary of 146 m, and 300 s be used as a critical time window for coordinated evacuation between the plant area and surrounding residential

Academic Editor: Zheng Sun

Received: 25 June 2026
Revised: 10 July 2026
Accepted: 22 July 2026
Published: 23 July 2026

areas. The findings provide a technical basis for safety-distance verification, monitoring layout design, and emergency-plan development for ground injection systems in oilfield CCUS projects.

Keywords: CCUS; CO_2 leakage; PHAST; KFX; risk zoning; emergency evacuation

1. Introduction

Carbon Capture, Utilization, and Storage (CCUS) is an important technological pathway for the low-carbon use of fossil energy and deep decarbonization of the petrochemical industry. With the continued advancement of China's dual-carbon goals, CCUS is shifting from single-point demonstration toward large-scale and clustered deployment. CO_2-enhanced oil recovery and storage has become a major engineering application route for CCUS in China because it can both improve oil recovery and enable geological storage [1–3]. According to projections by the Intergovernmental Panel on Climate Change (IPCC) [4], CCUS could contribute 0.1–0.4 Gt of CO_2 emission reductions per year by 2030 and 3.0–6.8 Gt per year by 2050. Assessments conducted by domestic research teams for China's carbon-neutrality pathway indicate that, under the 2060 net-zero scenario, CCUS could reduce annual emissions by 1.041 Gt, with a cumulative contribution of 14.6% [5]. According to the China CCUS Progress Report Series 2025, driven by the dual-carbon goals, China's CCUS development has entered a new stage of scaled demonstration. By July 2024, approximately 120 CCUS projects had been planned or put into operation in China, with a total capture capacity of about 6 million tons per year, covering power, steel, cement, chemical, and other industries. At the policy level, CCUS has been incorporated into China's "1 + N" policy framework for carbon peaking, and the concept of "building a batch of zero-carbon industrial parks" was first proposed at the Central Economic Work Conference, further strengthening the strategic role of CCUS in regional low-carbon development. In the field of CO_2-enhanced oil recovery and storage, China has relatively favorable source–sink matching conditions and a strong engineering implementation basis, which can support large-scale CO_2 emission reduction and promote the coordinated development of CO_2 capture, transport, injection, storage, and monitoring.

Although CO_2 is not a flammable or explosive medium, high-concentration leakage can threaten human life through oxygen displacement, asphyxiation, and toxicity. Once liquid or dense-phase CO_2 leaks from tanks, valves, pumps, or connecting pipelines, its dispersion process is affected not only by the leak aperture, tank pressure, ambient temperature, and wind speed but also by site buildings, equipment arrangements, and near-ground topographic conditions. The resulting accident consequences are sudden, difficult to perceive, and dynamically evolving [6,7]. Therefore, reliance on a single safety distance or static cordon is insufficient for emergency response at oilfield CCUS injection stations. Although relatively systematic safety assessment and regulatory requirements have been established abroad for CO_2-EOR and CCS projects, leakage risk zoning, monitoring-point layout, and emergency coordination rules for CO_2 flooding and ground injection systems in China still require further refinement. Quantitative consequence simulations under realistic site conditions are therefore urgently needed.

Existing studies on CO_2 leakage dispersion and risk assessment have mainly focused on source terms for CO_2 pipeline leakage, multiphase-flow phase transition, jet dispersion, leakage pathways in geological storage, and far-field migration. PHAST, CFD models, risk matrices, machine learning prediction, and multisensor monitoring have gradually been introduced into consequence assessment for CO_2 leakage. Shang et al. [8] systematically reviewed experiments and numerical simulations covering the full process of CO_2 pipeline leakage, compared different equations of state, leakage models, and numerical methods, and suggested that CFD simulations are more realistic, although studies on buried pipelines remain limited and method-oriented reviews still lack validation of emerging technologies. Sori [9] focused on experiments and simulations related to geological CO_2 storage and discussed subsurface diffusion behavior and storage stability but did not examine leakage risk and emergency response in detail. Li et al. [10] identified key scientific challenges related to CO_2 leakage risk assessment, storage-site stability, and monitoring technologies and highlighted the need to develop multiphysics-coupled leakage risk simulation systems. Li et al. [11] discussed industrial-scale experiments, CFD models, and risk assessment and identified machine learning prediction of CO_2 dispersion behavior as a future research direction. Tan et al. [12] analyzed the effects of top-hole aperture, impurities, and leakage direction on phase state, pressure, and temperature distributions in pipelines; verified the applicability of equations of state and multiphase-flow models; and noted that most buried-pipeline experiments involve pipe diameters below 100 mm. Future work should consider industrial-scale experiments, complex terrain, and irregular cracks. Yang et al. [13] conducted industrial-scale pipeline leakage experiments and analyzed impurity concentration diffusion and cloud morphology evolution in the jet region after dense-phase CO_2 leakage containing impurities, providing new evidence for large-scale far-field leakage assessment. For repurposed pipelines, Yang et al. [14] quantitatively evaluated the risk of converting in-service oil and gas pipelines for CO_2 transport, offering a new perspective for pipeline reuse, although the effects of CO_2 impurities, long-term aging, and field validation remain insufficiently addressed. In terms of risk assessment methods, Hu et al. [15] proposed a CO_2 leakage risk assessment method based on pipeline failure-probability correction and used PHAST to predict dispersion distances and risks, but extreme weather and complex terrain were not fully considered. Zhang et al. [16] developed an integrated framework of "threshold impact–distance calculation–risk matrix mapping" based on PHAST simulations, constructed 4320 scenarios, calculated the impact distances for 1%, 4%, and 10% concentration thresholds, mapped the results into five risk levels, used XGBoost for modeling, and proposed graded control through "risk level plus multi-threshold annuli". Chen et al. [17] proposed a dynamic risk assessment framework for long-term geological storage, supporting real-time monitoring but lacking specific application cases and data validation. In monitoring technology, Saini et al. [18] proposed a hybrid monitoring framework based on computer vision and multisensor fusion, improving early leak detection accuracy and real-time response capability.

The PHAST-KFX two-stage simulation framework explicitly clarifies that no dynamic data exchange or iterative feedback exists between the two software platforms. Instead, the two approaches achieve complementary advantages through a sequential workflow consisting of multi-scenario screening, three-dimensional validation under representative scenarios, and risk zoning assessment. The main innovations of this study are summarized as follows:

(1) Methodological innovation

Previous studies have mainly relied on either standalone PHAST simulations for rapid consequence screening or standalone CFD simulations (e.g., FLUENT) for detailed dispersion analysis. However, PHAST alone cannot capture the influence of complex site-specific buildings and equipment layouts on near-ground airflow patterns and gas cloud accumulation, whereas standalone CFD simulations are computationally intensive and inefficient for large-scale multi-scenario screening.

The proposed PHAST-KFX framework integrates the advantages of both approaches: PHAST enables rapid screening of multiple leakage scenarios to identify critical conditions, while KFX provides detailed three-dimensional dispersion analysis for these representative scenarios by incorporating site-specific building and equipment effects. This two-stage framework achieves a balance between computational efficiency and simulation accuracy, which has rarely been demonstrated for ground injection systems in oilfield CCUS facilities.

(2) Scenario-oriented contribution

Although most existing studies have focused on pipeline leakage or geological storage-related CO_2 release scenarios [19], this study specifically investigates liquid CO_2 leakage from storage tanks located within oilfield ground injection stations. This scenario is highly relevant to operational safety but has received relatively limited attention in previous research.

(3) Practical engineering contribution

Unlike previous studies that mainly reported impact distances or low-concentration dispersion boundaries, this study establishes a complete engineering workflow from consequence simulation, high-concentration risk zoning, and risk quantification to emergency control strategies, including monitoring layout, safety exclusion boundaries, and evacuation time windows. This framework provides directly applicable support for site-specific emergency planning and safety management of oilfield CCUS facilities.

On this basis, the present study investigates leakage from a liquid CO_2 storage tank at an oilfield CO_2 cyclic injection station, focusing on leakage dispersion and risk control for a ground injection system under high-pressure, low-temperature, and complex site conditions. A 1:1 two-dimensional and three-dimensional site model was established, and coupled PHAST-KFX simulations were performed. Different combinations of leak aperture, ambient temperature, and wind speed were first configured to identify the dispersion range, concentration distribution, duration, and source-term evolution following liquid CO_2 leakage. High-concentration CO_2 toxicity thresholds and the risk quantification method were then used to characterize leakage-affected areas by risk level and quantify risks at different distances. Finally, control recommendations were proposed for monitoring and alarm systems, warning boundaries, and emergency coordination. The study aims to provide a site-specific technical basis for consequence assessment, safety-distance verification, and emergency-plan optimization for ground injection systems in oilfield CCUS projects.

2. PHAST-KFX Two-Stage Simulation Framework

2.1. Methodological Framework

2.1.1. Methodology Description

In this study, a PHAST-KFX two-stage simulation framework was developed to investigate the risk characteristics of CO_2 leakage dispersion. It should be noted that this framework does not involve dynamic data exchange or iterative feedback between the two software platforms; rather, it represents a staged analysis approach for engineering accident consequence assessment.

In the first stage, PHAST (version 9.1, DNV, Høvik, Norway) was employed to perform multi-scenario consequence screening. By varying key influencing parameters, including leakage aperture size, ambient temperature, and wind speed, different accident scenarios were evaluated to obtain the CO_2 leakage source terms, dispersion distances, concentration threshold ranges, and maximum cloud coverage areas. Based on these results, representative high-risk scenarios were identified for further analysis.

In the second stage, KFX(version 4.0.29, DNV, Høvik, Norway) was applied to establish three-dimensional site-specific models containing major buildings, equipment, and spatial layouts for the representative high-risk scenarios selected from the PHAST analysis. Under consistent conditions of leakage medium, leakage aperture, storage tank state, ambient conditions, and wind field parameters, KFX was further used to investigate the effects of building obstruction, equipment-induced flow disturbance, near-ground accumulation, and complex spatial configurations on CO_2 cloud dispersion behavior.

Through this two-stage framework, PHAST is responsible for rapid multi-scenario screening, while KFX provides detailed three-dimensional dispersion analysis under complex site conditions. The two approaches complement each other by integrating computational efficiency with physical representation of site-specific dispersion characteristics. The detailed input parameters and output variables of the two models are summarized in Table 1.

Table 1. Functional division and output metrics of the PHAST-KFX coupled simulation.

Software/Module	Main Function	Key Inputs	Main Outputs
PHAST	Rapid multi-scenario consequence assessment	Leak aperture; tank pressure and temperature; ambient temperature; wind speed; atmospheric stability; concentration thresholds	Maximum dispersion range; concentration-threshold distance; cloud footprint; leakage duration
KFX	Three-dimensional dispersion simulation in complex stations	Three-dimensional station model; leakage-source location; wind direction and speed; building and equipment layout; monitoring points	Gas-cloud spatiotemporal evolution; near-ground accumulation; building bypass flow; coverage time of key areas
Risk assessment	Safety zoning and emergency management	Toxicity thresholds; impact distances; risk values; exposure scenarios	Risk zones; monitoring layout; warning boundary; emergency coordination time window

The specific simulation procedure is as follows: First, a leakage scenario matrix is established based on site layout information, storage tank operating parameters, and local meteorological conditions. Second, PHAST is employed to calculate the maximum dispersion range, maximum concentration distance, and influence areas corresponding to different concentration thresholds under various accident scenarios. Third, representative high-risk scenarios are selected and further analyzed using the KFX three-dimensional model to characterize CO_2 cloud migration pathways among site buildings, accumulation in low-lying areas, and spatial coverage at critical time points. Finally, high-concentration risk zones are determined by integrating CO_2 toxicity thresholds and risk quantification methods, and corresponding recommendations for monitoring layout, safety boundaries, and emergency evacuation are proposed.

2.1.2. Governing Equations and Physical Mechanisms

The CO_2 leakage and dispersion process is characterized as an unsteady multicomponent flow problem involving mass, momentum, energy, and species transport with source terms. In this study, PHAST is employed for rapid consequence assessment, including the estimation of leakage source terms, dispersion distances, and toxic impact ranges under multiple release scenarios [20–27]. Meanwhile, KFX is used to perform three-dimensional transient CFD simulations for representative high-risk scenarios, considering the effects of complex site geometry, equipment arrangement, atmospheric conditions, and near-ground accumulation on CO_2 dispersion behavior [28–33].

In the KFX-based three-dimensional simulations, the CO_2–air mixture is considered a compressible multicomponent fluid. The governing equations describing the transport processes can be generally expressed in terms of the conservation of mass, momentum, energy, and species concentration, as follows:

(1) Mass conservation equation:

$\partial\rho/\partial t + \nabla\cdot(\rho u) = S\_m;$

(2) Momentum conservation equation:

$\partial(\rho u)/\partial t + \nabla\cdot(\rho uu) = -\nabla p + \nabla\cdot\tau\_eff + \rho g + S\_u;$

(3) Energy conservation equation:
$\partial(\rho h)/\partial t + \nabla\cdot(\rho u h) = \partial p/\partial t + \nabla\cdot(\lambda\_eff \nabla T) + \Phi + S\_h$;
(4) CO_2 species transport equation:
$\partial(\rho Y\_CO_2)/\partial t + \nabla\cdot(\rho u Y\_CO_2) = \nabla\cdot(\rho D\_eff \nabla Y\_CO_2) + S\_CO_2$

ρ represents the density of the CO_2–air mixture, u is the velocity vector, p is the pressure, τ_eff represents the effective viscous stress tensor, g denotes gravitational acceleration, h is the specific enthalpy, T is the temperature, λ_eff is the effective thermal conductivity, Φ represents viscous dissipation, YCO_2 is the mass fraction of CO_2, and D_eff is the effective diffusion coefficient. Sm, Su, Sh, and S_CO_2 represent the source terms of mass, momentum, energy, and species transport, respectively. When turbulent diffusion is considered, the effective diffusion coefficient can be expressed as follows:

$$D_{eff} = D_m + \frac{\mu_t}{\rho Sc_t}$$

Dm is the molecular diffusion coefficient, μ_t represents the turbulent viscosity, and Sc_t denotes the turbulent Schmidt number.

For the PHAST calculations, this study does not treat PHAST as a full three-dimensional CFD solver. Instead, PHAST is employed to determine leakage source terms and consequence parameters, including release rates, leakage durations, concentration impact distances, and toxic consequence ranges under different accident scenarios.

The leakage source term of the storage tank can be generally described by the overall mass and energy conservation relationships:

$$\frac{\mathrm{dM_{tank}}}{\mathrm{dt}} = -\dot{\mathrm{m}}_{\mathrm{leak}}$$

$$\frac{\mathrm{dU_{tank}}}{\mathrm{dt}} = -\dot{\mathrm{m}}_{\mathrm{leak}}\mathrm{h}_{\mathrm{leak}} + \mathrm{Q}$$

where $\mathrm{M_{tank}}$ and $\mathrm{U_{tank}}$ represent the mass and internal energy of the stored medium, respectively; $\dot{\mathrm{m}}_{\mathrm{leak}}$ denotes the leakage mass flow rate; $\mathrm{h_{leak}}$ represents the specific enthalpy of the released fluid; and Q represents the heat transfer from the surroundings. For short-duration accident consequence simulations, Q can be treated as either an adiabatic condition or a finite heat transfer term depending on the model settings.

It should be noted that CO_2 dispersion is not governed solely by molecular diffusion. During the leakage process, high-speed jet momentum, atmospheric wind fields, and site-specific buildings and equipment can induce significant turbulent mixing, flow obstruction, recirculation, and local accumulation. In the PHAST stage, atmospheric dispersion and dilution effects are represented through input parameters such as wind speed, atmospheric stability, ambient temperature, and relative humidity. In the KFX stage, three-dimensional transient CFD simulations are performed to further characterize flow structures, turbulent mixing, near-ground recirculation, and local CO_2 accumulation under complex site conditions. For CO_2 species transport, the effective diffusion coefficient can be expressed as the combined contribution of molecular and turbulent diffusion:

$$D_{eff} = D_m + \frac{\mu_t}{\rho Sc_t}$$

where D_{eff} represents the effective diffusion coefficient, D_m is the molecular diffusion coefficient, μ_t is the turbulent viscosity, ρ is the mixture density, and Sc_t is the turbulent Schmidt number.

Therefore, the evolution of the CO_2 concentration field is simultaneously governed by mean-flow convection, molecular diffusion, and turbulent diffusion. In this study, no additional modification or secondary development of the internal turbulence closure models in KFX was performed; instead, turbulent transport was treated using the built-in numerical solution framework of the software.

2.2. Accident Scenario and Boundary Conditions

2.2.1. Selection of Accident Scenario

In this study, a liquid CO_2 storage tank leakage scenario caused by tank overfilling or pressure control system failure was selected as the representative high-risk accident scenario. The selection of this scenario was primarily based on the operational characteristics of oilfield CCUS ground injection systems and the principles of accident consequence assessment, rather than on a single accident probability statistic.

The criteria for scenario selection are as follows:

(1) Operational experience:

Based on the operational experience of the PetroChina Liaohe Oilfield Company, liquid CO_2 storage tank overfilling and pressure relief valve failure were identified as highly credible, high-consequence scenarios.

(2) Regulatory requirements:

According to GB/T 37243-2019 [34], scenarios involving storage tank overfilling and pressure control failure should be considered in quantitative risk assessments of hazardous chemical storage facilities.

(3) Consequence severity:

Compared with small-scale pipeline leakage, storage tank leakage involves a larger release inventory (150 m^3), higher initial pressure (2.8 MPa), more complex phase-transition processes, and a wider potential impact range. After release, liquid CO_2 undergoes rapid depressurization, flash evaporation, dry ice formation, and heavy gas dispersion processes. Under the influence of site buildings and equipment layouts, the released CO_2 cloud may accumulate near the ground and form localized high-concentration regions.

Therefore, this scenario was selected as a representative high-risk condition to investigate CO_2 leakage dispersion characteristics, high-concentration risk zones, and emergency response time, providing a technical basis for the safety assessment of CCUS ground injection facilities.

2.2.2. Boundary Conditions and Parameter Determination

The leaking medium was liquid CO_2. The storage tank volume was 150 m^3, the medium temperature was −20 °C, and the pressure was 2.8 MPa. The leakage direction was set to (0.5, 0.5, 0); the prevailing wind direction was 270° (westerly wind); atmospheric stability was class D (neutral); and relative humidity was 66%. Monitoring heights were set to 1.7 m and 0.66 m to represent breathing-zone exposure and near-ground accumulation, respectively. According to the leak-aperture classification criteria in GB/T 37243-2019, three apertures were selected: 5 mm (small leak), 25 mm (medium leak), and 50 mm (large leak). Meteorological parameters included the local average temperature of the coldest month (−11.2 °C), the average temperature of the hottest month (24.5 °C), the minimum wind speed (1.5 $m \cdot s^{-1}$), the annual average wind speed (4.6 $m \cdot s^{-1}$), and the maximum wind speed (28 $m \cdot s^{-1}$). The averaging time for the simulations was set to 900 s to describe the influence range during the initial accident stage and the process approaching a quasi-steady dispersion state.

(1) Rationale for Selecting the 0.66 m Monitoring Height

a. Equipment-specific considerations:

At the Liaohe Oilfield CO_2 injection station, several critical components and maintenance points associated with key equipment (including the bottom platforms of hydrocarbon removal adsorption towers and the lower sections of storage tank supports) are located approximately 0.6–0.7 m above the ground. Leakage occurring at these locations is expected to result in CO_2 accumulation and detection at this height.

b. Human posture considerations:

During emergency response operations, personnel may adopt crouching or crawling postures to reduce exposure to high-concentration CO_2 regions, as CO_2 is denser than air and tends to accumulate near the ground. Therefore, the 0.66 m height approximately represents the breathing zone of an adult in a crouched posture (approximately 0.6–0.7 m).

c. Topographical considerations:

The site contains small-scale, low-lying areas (approximately 0.1–0.3 m depressions), where dense CO_2 tends to accumulate due to gravity-driven stratification. The 0.66 m monitoring height represents the upper boundary of the near-ground accumulation layer, allowing the potential accumulation characteristics of heavy CO_2 clouds to be evaluated.

Monitoring Height Sensitivity Analysis:

A sensitivity analysis was conducted to evaluate the influence of monitoring height on the boundaries of risk zones. Three additional monitoring heights (0.3 m, 1.0 m, and 2.0 m) were analyzed, as summarized in Table 2.

Table 2. Sensitivity analysis results of different monitoring heights.

Monitoring Height (m)	10% CO_2 Concentration Boundary (m)	30% CO_2 Concentration Boundary (m)
0.3	38	14
0.66	35	13
1.0	32	12
1.7	28	11
2.0	26	10

The results indicate that the difference between the 0.66 m and 1.7 m monitoring heights is approximately 7 m for the 10% concentration boundary and approximately 2 m for the 30% concentration boundary. Compared with the 1.7 m breathing-zone height, the 0.66 m monitoring height provides a more conservative estimation (i.e., a larger hazardous zone), which is appropriate for safety assessment.

(2) Basis for Leakage Aperture Selection

The leakage apertures (5 mm, 25 mm, and 50 mm) were selected according to the leakage hole classification criteria specified in GB/T 37243-2019, Determination Method of External Safety Protection Distance for Hazardous Chemical Production Units and Storage Facilities.

According to this standard:

a. The 5 mm leakage aperture represents a small-hole leakage scenario, which is typically associated with pinhole corrosion, sealing failure, or minor flange leakage.

b. The 25 mm leakage aperture represents a medium-hole leakage scenario, corresponding to failures such as valve stem malfunction, gasket rupture, or moderate pipeline damage.

c. The 50 mm leakage aperture represents a large-hole leakage scenario, approaching a complete rupture of a small-diameter connection pipe.

These three leakage categories collectively cover credible leakage scenarios associated with storage tank connections, valves, and flanges in oilfield CO_2 injection stations, providing representative conditions for consequence assessment.

(3) Basis for Leakage Direction Selection

The leakage direction was set as (0.5, 0.5, 0). The vertical component is zero, indicating that the leakage jet is primarily located within the horizontal plane. The two equal horizontal components represent an inclined release direction relative to the site coordinate system. This configuration is used to approximate a typical lateral leakage scenario caused by damage to liquid CO_2 storage tank connection pipes, valve assemblies, flanges, or pipeline connections. Since the spatial orientation of the leakage orifice can significantly affect the initial trajectory of the high-speed jet, momentum dissipation, near-field concentration distribution, and flow interactions between buildings and equipment, the three-dimensional dispersion pathways, station coverage time, and risk boundaries obtained in this study are mainly applicable to the selected leakage orientation.

(4) Basis for Meteorological Parameter Selection

Wind speed (1.5, 4.6, and 28 $m \cdot s^{-1}$): The selected wind speeds represent the minimum wind speed, annual average wind speed, and maximum wind speed at the specific site, respectively, based on local meteorological station records from 1981 to 2020. The 1.5 $m \cdot s^{-1}$ condition represents the most unfavorable dispersion scenario, characterized by weak atmospheric dilution and a higher tendency for near-field CO_2 accumulation. The 28 $m \cdot s^{-1}$ condition represents an extreme wind condition that may enhance downwind transport and increase the affected distance of the CO_2 cloud.

Temperature (−11.2 °C and 24.5 °C): The selected temperatures correspond to the average temperature of the coldest month (January) and the average temperature of the hottest month (July) at the study site, based on the same meteorological records. These two boundary conditions represent the seasonal operating temperature range and account for the influence of temperature variation on liquid CO_2 leakage behavior and dispersion characteristics.

Atmospheric stability (Class D, neutral condition): The Class D atmospheric stability condition was selected because it represents the most frequently occurring meteorological condition at the study site according to local meteorological statistics, accounting for approximately 60% of the annual occurrence frequency. The corresponding meteorological conditions provide a representative atmospheric environment for evaluating CO_2 dispersion behavior under typical operational conditions.

The basis and sources of all input parameters are summarized in Table 3.

Table 3. Basis and sources of simulation input parameters.

Parameter	Value	Source/Rationale
Storage tank volume	150 m^3	Actual specification of the CO_2 storage tank at the Liaohe Oilfield injection station
Medium temperature	−20 °C	Actual operating temperature of the liquid CO_2 storage tank (maintained at −20 °C to keep CO_2 in liquid state at 2.8 MPa)
Tank pressure	2.8 MPa	Actual operating pressure of the storage tank (saturation pressure of CO_2 at −20 °C)
Leak aperture	5, 25, 50 mm	GB/T 37243-2019 classification
Ambient temperature	−11.2 °C, 24.5 °C	Local meteorological records (1981–2020): January average and July average
Wind speed	1.5, 4.6, 28 $m \cdot s^{-1}$	Local meteorological records: minimum, annual average, and maximum wind speeds
Wind direction	270° (westerly)	Local prevailing wind direction from meteorological records
Atmospheric stability	Class D (neutral)	Most frequent stability class at the site (~60% of the year)

Note: All site-specific parameters (including storage tank volume, temperature, pressure, and meteorological conditions) were obtained from the actual design and operational data of the Liaohe Oilfield CO_2 cyclic injection station and were used with permission from the operating company. Meteorological data were obtained from local weather station records covering the period from 1981 to 2020.

2.2.3. Data Sources

1. Data sources for the three-dimensional site model:

Primary source:

The as-built engineering drawings of the Liaohe Oilfield CO_2 cyclic injection station provided by PetroChina Liaohe Oilfield Company were used as the primary data source. The site geometry was constructed at a 1:1 scale to accurately represent the spatial arrangement of major buildings and equipment.

Secondary source:

Field measurements were conducted by the research team in June 2025, including photographic documentation and dimensional verification of key buildings and equipment, to validate the geometric parameters used in the model.

Tertiary source:

Satellite imagery from Google Earth was used to verify the overall site layout and spatial distribution of the facility.

2. Geometric model simplification principles

Buildings and major equipment:

All major structures, including storage tanks, adsorption towers, control rooms, electrical cabinet rooms, and large-scale equipment, were modeled using geometric primitives (rectangular blocks or cylindrical structures) while maintaining their actual dimensions (height, width, and depth). Roof structures were simplified as flat surfaces.

Small pipelines and minor components:

Pipelines and small-diameter pipes with diameters smaller than 50 mm were not explicitly modeled because their blockage ratio was considered negligible (<2% of the total facility volume), and their influence on large-scale dispersion patterns was limited.

Overall, the model maintained high geometric fidelity by preserving the actual dimensions and spatial locations of major buildings and equipment, while secondary details with negligible influence on flow characteristics, such as small pipes, cable trays, and handrails, were appropriately simplified.

3. Equipment blockage ratio

The total blockage ratio of all modeled objects was approximately 8–12% of the total station volume, which is consistent with recommended practices for CFD-based dispersion modeling of industrial facilities.

4. Model resolution and grid independence verification

The computational domain was discretized using structured hexahedral meshes, with local mesh refinement applied near the leakage source and major buildings/equipment. Grid independence was evaluated using three different mesh resolutions: coarse mesh: approximately 1.2 million cells; medium mesh: approximately 2.8 million cells (selected for all simulations); fine mesh: approximately 5.6 million cells. The maximum difference in CO_2 concentration predictions between the medium and fine meshes was less than 3.5%, confirming that the selected mesh resolution was sufficiently independent and reliable for subsequent simulations.

2.3. Concentration Thresholds and Risk Assessment Indicators

The risk assessment of CO_2 leakage accidents cannot be determined solely based on a single concentration threshold. Instead, it should comprehensively consider gas concentration, exposure duration, and human response characteristics. Therefore, based on the toxicological effects of CO_2 and engineering emergency management requirements, the concentration thresholds in this study are classified into two categories: safety monitoring thresholds and high-concentration acute injury thresholds.

The threshold values were determined based on multiple authoritative sources, including occupational exposure standards and toxicological risk assessment methods.

(1) National Institute for Occupational Safety and Health (NIOSH)

According to the guidelines provided by the National Institute for Occupational Safety and Health (NIOSH):

Time-weighted average (TWA): 5000 ppm (0.5%), corresponding to an 8 h exposure limit.

Short-term exposure limit (STEL): 30,000 ppm (3%), corresponding to a 15 min exposure limit.

Immediately Dangerous to Life or Health (IDLH): 40,000 ppm (4%).

(2) Chinese Occupational Exposure Standards

According to GBZ 2.1-2019 [35], Occupational Exposure Limits for Hazardous Agents in the Workplace—Part 1: Chemical Hazardous Agents, the permissible concentration–time weighted average (PC-TWA) is 9000 mg/m^3 (approximately 5000 ppm).

Permissible short-term exposure concentration (PC-STEL): 18,000 mg/m^3 (approximately 10,000 ppm).

(3) HSE Dangerous Toxic Load (DTL) Method

According to the Dangerous Toxic Load (DTL) methodology proposed by the UK Health and Safety Executive (HSE), toxic effects are evaluated by considering both concentration and exposure duration.

The DTL concept can be expressed as follows:

$$DTL = C^n \times t$$

C represents the gas concentration; n represents the toxicity exponent (for CO_2, commonly assumed as n = 1); t represents the exposure duration.

This indicates that the adverse health effects of CO_2 exposure depend not only on the concentration level but also on the duration of exposure.

Based on the above standards and toxicological criteria, Table 4 summarizes the physiological responses of humans under different CO_2 concentration levels and exposure durations.

Table 4. Effects of different CO_2 volume concentrations on human health.

CO_2 Content in Air/vol %	Effect on Humans	CO_2 Content in Air/vol %	Effect on Humans
1–1.5	Chest tightness, dizziness, increased heart rate, and mild metabolic interference	15	Unconsciousness within 1 min; CO_2 begins to irritate mucous membranes
3	Mild narcosis, dyspnea, elevated blood pressure, and increased heart rate	20	Most victims lose the ability to escape; fatalities begin to occur
4–5	Dyspnea, panting, headache, dizziness, and aggravated poisoning after 30 min	30	Loss of consciousness within 30 s; fainting within 1 min; most individuals die
7	Marked discomfort, dizziness, and impaired hearing and vision	>30	Fainting within 30 s followed by death; very few individuals may survive and recover
10	Respiration becomes increasingly rapid; escape ability remains initially, but consciousness is soon lost		

The first category is the safety monitoring and alarm threshold. In this study, CO_2 volume fractions of 3%, 5%, 7%, and 10% were selected as monitoring concentration levels, which were used to identify the dispersion range of the gas cloud, determine alarm trigger conditions, and assist in defining personnel evacuation zones. These thresholds are primarily applied for early accident detection and risk warning, rather than representing long-term occupational exposure limits.

The second category is the high-concentration acute injury threshold. In this study, CO_2 volume fractions of 10%, 15%, 20%, and 30% were selected as the criteria for risk zoning to classify areas with different levels of acute injury risks. Specifically:

The 10% concentration zone represents a high-concentration exposure area, where access by non-essential personnel should be restricted.

The 15% concentration zone represents a severe injury risk area, where short-term exposure may result in significant physiological effects.

The 20% concentration zone represents an extremely high-risk area, where entry is only permitted for professionally trained personnel equipped with appropriate protective equipment.

The 30% concentration zone represents a fatal-risk area, where personnel entry should be strictly prohibited.

It should be noted that the hazards associated with CO_2 exposure are jointly determined by gas concentration and exposure duration. Therefore, this study adopts the concentration–time–human response relationship as the theoretical basis for risk assessment and combines the maximum impact range during the leakage process to establish conservative risk zones. During actual emergency response, safety boundaries should be dynamically adjusted based on real-time CO_2 concentration monitoring results and personnel exposure duration.

3. Leakage Dispersion Results and Mechanistic Discussion

The two-dimensional PHAST software can simulate the maximum dispersion range and maximum concentration distance for CO_2 leakage under different operating conditions, whereas the three-dimensional KFX software can monitor the dispersion process in real time, determine the maximum dispersion time for the gas cloud to cover the entire CO_2 cyclic injection station, and analyze leakage-rate variations through monitoring points. Therefore, the two tools were combined in this study to comprehensively analyze the consequences of CO_2 storage-tank leakage.

To analyze the effects of different parameters on CO_2 leakage and dispersion behavior, sensitivity analyses were conducted in this study considering three key factors: leakage aperture size, ambient temperature, and wind speed. Among these factors, the leakage aperture size primarily affects the leakage source strength and initial jet momentum, making it a critical factor determining the overall accident consequence scale. The ambient temperature mainly influences the dispersion characteristics by altering the heat transfer conditions and phase-change behavior during liquid CO_2 leakage. The wind speed affects the migration pathway of the CO_2 cloud by changing atmospheric transport capacity and dilution effects.

3.1. Dominant Role of Leak Aperture in Dispersion Scale

The 900 s duration was selected as the engineering statistical time window for accident consequence assessment, primarily to cover the entire evolution process of liquid CO_2 leakage, including the initial jet dispersion stage, rapid gas cloud spreading within the station, near-ground accumulation, and the subsequent stabilization of the affected area. The KFX simulation results for the representative scenario show that, under the conditions of a 25 mm leakage aperture and an annual average wind speed of 4.6 $m \cdot s^{-1}$, the CO_2 cloud reaches the vicinity of the hydrocarbon removal adsorption towers at approximately 100 s, nearly covers the low-lying areas of the station at approximately 200 s, and approaches full coverage of the injection station with an outward expansion trend toward the site boundary at approximately 300 s. Meanwhile, the leakage rate at the monitoring point near the leakage source becomes relatively stable after approximately 20 s. Therefore, the 900 s simulation window is sufficient to capture the initial accident development stage and the formation process of the major impact boundaries. It should be noted that the 900 s duration is adopted as an engineering consequence assessment time window rather than a universal criterion indicating that all accident scenarios have reached a strict mathematical steady state.

https://doi.org/10.3390/pr14152383

The effects of different wind speeds, leak apertures, and temperatures on CO_2 dispersion after 900 s of leakage were compared. The maximum dispersion ranges under the considered operating conditions are listed in Table 5, and the cloud footprint is shown in Figure 1, using the case of −11.2 °C and a 5 mm leak aperture as an example.

Table 5. Maximum dispersion range under different operating conditions.

No.	Ambient Temperature/°C	Leak Aperture/mm	Maximum Dispersion Range/m	Maximum Cloud Footprint/m^2
1	−11.2	5	8.8	4.8
2	−11.2	25	41	123.8
3	−11.2	50	132	2204.1
4	24.5	5	9.4	5.4
5	24.5	25	48.5	180.8
6	24.5	50	146	2599.6

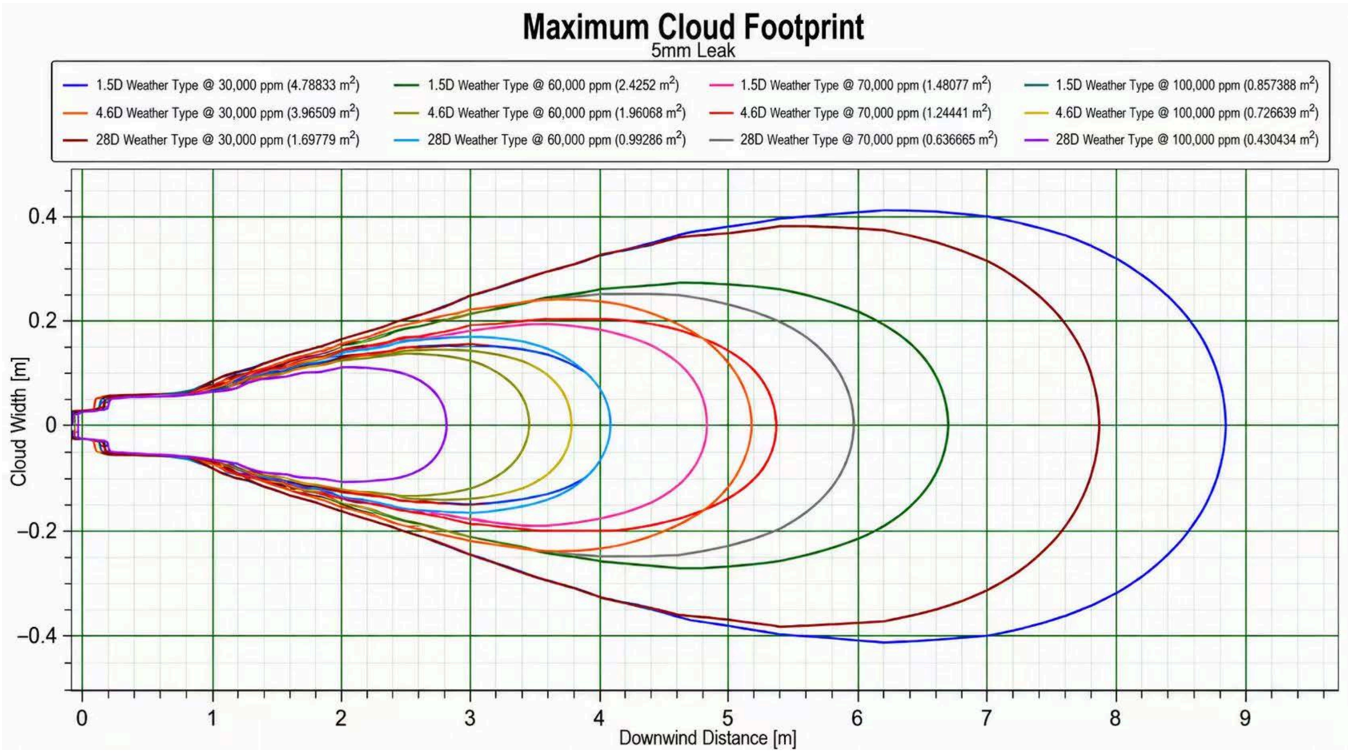

Figure 1. Maximum dispersion range at −11.2 °C and a 5 mm leak aperture.

The PHAST results show that the leak aperture is the dominant factor controlling the CO_2 dispersion range. Under identical meteorological conditions, increasing the aperture from 5 mm to 50 mm substantially increased the source-term strength and initial momentum, leading to nonlinear growth in both the maximum dispersion range and cloud footprint. Under the low-temperature condition (−11.2 °C), the maximum dispersion range increased from 8.8 m to 132 m. Under the higher-temperature condition (24.5 °C), it increased from 9.4 m to 146 m. The corresponding maximum cloud footprint increased from 4.8–5.4 m^2 to 2204.1–2599.6 m^2. For small-aperture leakage, the maximum hazard area remained closer to the leakage source; therefore, CO_2 concentration sensors should be densely installed around storage tanks, valve groups, and pipe racks, with sensor spacing in near-field key areas controlled within 10 m. For large-aperture leakage, rapid downwind boundary expansion and sensitive off-site receptors should be prioritized.

These results indicate that storage-tank nozzles, valves, flanges, and pipeline connections, where larger leak apertures may form, should be treated as key targets for integrity management and online monitoring. Compared with small leaks, large leaks have shorter durations but can generate larger high-concentration clouds within a short time, imposing higher requirements on rapid personnel evacuation and emergency response.

3.2. Effects of Temperature and Wind Speed on Near-Field Accumulation and Far-Field Transport

Temperature had a measurable influence on CO_2 dispersion. At higher temperatures, CO_2 volatility and dispersion capacity increased, making the maximum dispersion range under the 24.5 °C condition slightly larger than that under −11.2 °C. Under low-temperature conditions, gas density increases and molecular motion is restrained, weakening cloud dispersion capacity; however, dense-gas behavior becomes more pronounced, leading to near-ground transport and local accumulation.

Wind speed exhibited a dual effect of near-field dilution and far-field transport. At low wind speed (1.5 $m \cdot s^{-1}$), horizontal transport was weak, and CO_2 readily accumulated at high concentrations near the ground and in low-lying areas. At moderate wind speed (4.6 $m \cdot s^{-1}$), the near-field concentration peak decreased, but concentration attenuation in the mid- to far-field became slower. At high wind speed (28 $m \cdot s^{-1}$), the near-field concentration decreased further, but downwind transport accelerated, and short-term exposure risks at greater distances still required attention. Therefore, it should not be assumed that leakage risk necessarily decreases under strong-wind conditions; warning zones should be dynamically adjusted according to wind speed and wind direction.

3.3. Three-Dimensional Spatial Evolution and Emergency Action Time Window

The KFX three-dimensional simulation further revealed the influence of site buildings and equipment layout on gas-cloud dispersion paths. Under a 25 mm leak and an average wind speed of 4.6 $m \cdot s^{-1}$, the cloud initially spread outward from the leakage point, with release momentum dominating near-field dispersion. Over time, because CO_2 is denser than air, it gradually settled and spread along the ground surface, equipment gaps, and low-lying areas. Figure 2 shows cloud dispersion at 2, 10, 50, 100, 200, and 300 s.

The simulation results indicate that, from the perspective of leakage orientation, the representative scenario considered in this study involves a horizontal oblique leakage jet. During the initial stage of CO_2 leakage, the gas cloud spreads outward from the leakage point under the influence of airflow, and the leakage rate is relatively high, with momentum dominating the dispersion process. As the leakage continues, CO_2 exhibits heavy gas characteristics due to its higher density than air, resulting in ground-hugging dispersion and local accumulation on the ground surface, within equipment gaps, and in low-lying areas. Under the horizontal oblique leakage scenario, the influence of building and equipment layouts on the gas cloud dispersion pathway becomes more pronounced, leading to flow diversion, recirculation, and local high-concentration regions behind equipment, within narrow passages, and near-ground spaces. Approximately 100 s after leakage, the CO_2 cloud can disperse to the vicinity of six hydrocarbon removal adsorption towers and extend toward the control room and electrical cabinet room; at approximately 200 s, the gas cloud has basically covered the low-lying ground areas of the station, posing a direct threat to near-ground operating personnel; at approximately 300 s, the gas cloud approaches coverage of the entire CO_2 injection station and exhibits a tendency to expand beyond the facility boundary. Therefore, 300 s can be considered an important time window for initial plant evacuation and coordinated emergency response with surrounding residential areas. It should be emphasized that the 300 s evacuation/control time window is a simulation result under the specific site conditions, including the specific meteorological conditions (annual average wind speed of 4.6 m·s^{-1}, leakage aperture of 25 mm, and temperature of −11.2 °C) and the current station layout. This value should not be regarded as a universal recommendation. In practical emergency response plans, it should be used as a control indicator, requiring the completion of alarm activation, process shutdown, personnel evacuation, and external emergency coordination before this time. Under unfavorable conditions such as sudden wind direction changes, nighttime low temperatures, snowfall, or stagnant wind conditions, earlier actions should be taken.

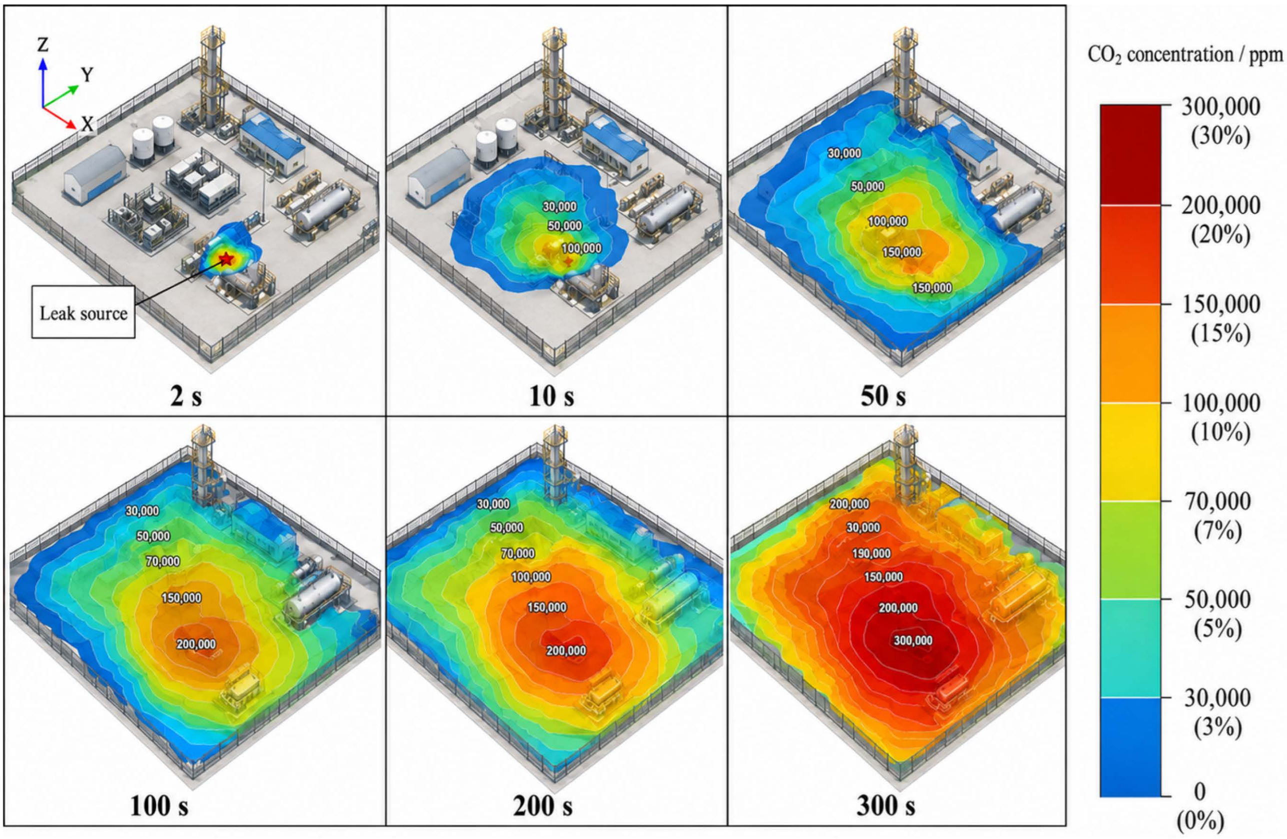

Figure 2. Spreading distribution of CO_2 leakage at different times.

The KFX three-dimensional simulation results further demonstrate that the arrangement of buildings and equipment within the station significantly affects the local flow structures of the leaked gas cloud. During the initial leakage stage, the CO_2 jet exhibits strong initial momentum, and turbulent mixing mainly occurs near the leakage source and within the jet shear layer. As leakage continues, the gas cloud is affected by both the ambient wind field and obstacles, resulting in flow diversion, recirculation, and local accumulation within equipment gaps, the wake regions behind buildings, and near-ground areas. Due to the higher density of CO_2 compared with air, turbulent mixing can promote near-field dilution; however, high-concentration accumulation may still occur in low-lying areas and poorly ventilated regions. Therefore, the application of KFX three-dimensional simulations helps overcome the limitations of conventional two-dimensional consequence assessment software, which cannot adequately capture complex site-specific effects such as turbulent flow around structures and near-ground accumulation of heavy gases.

3.4. *Effect of Phase Transition on Leakage Rate and Sealing Timing*

Based on the equipment layout of the CO_2 injection station, 18 concentration monitoring points were arranged at a height of 0.66 m above ground. Using the KFX three-dimensional simulation results and monitoring-point data for CO_2 storage-tank leakage,

https://doi.org/10.3390/pr14152383

leakage-rate variations were analyzed. Four monitoring points near the leakage location were selected, and their leakage-rate curves are shown in Figure 3.

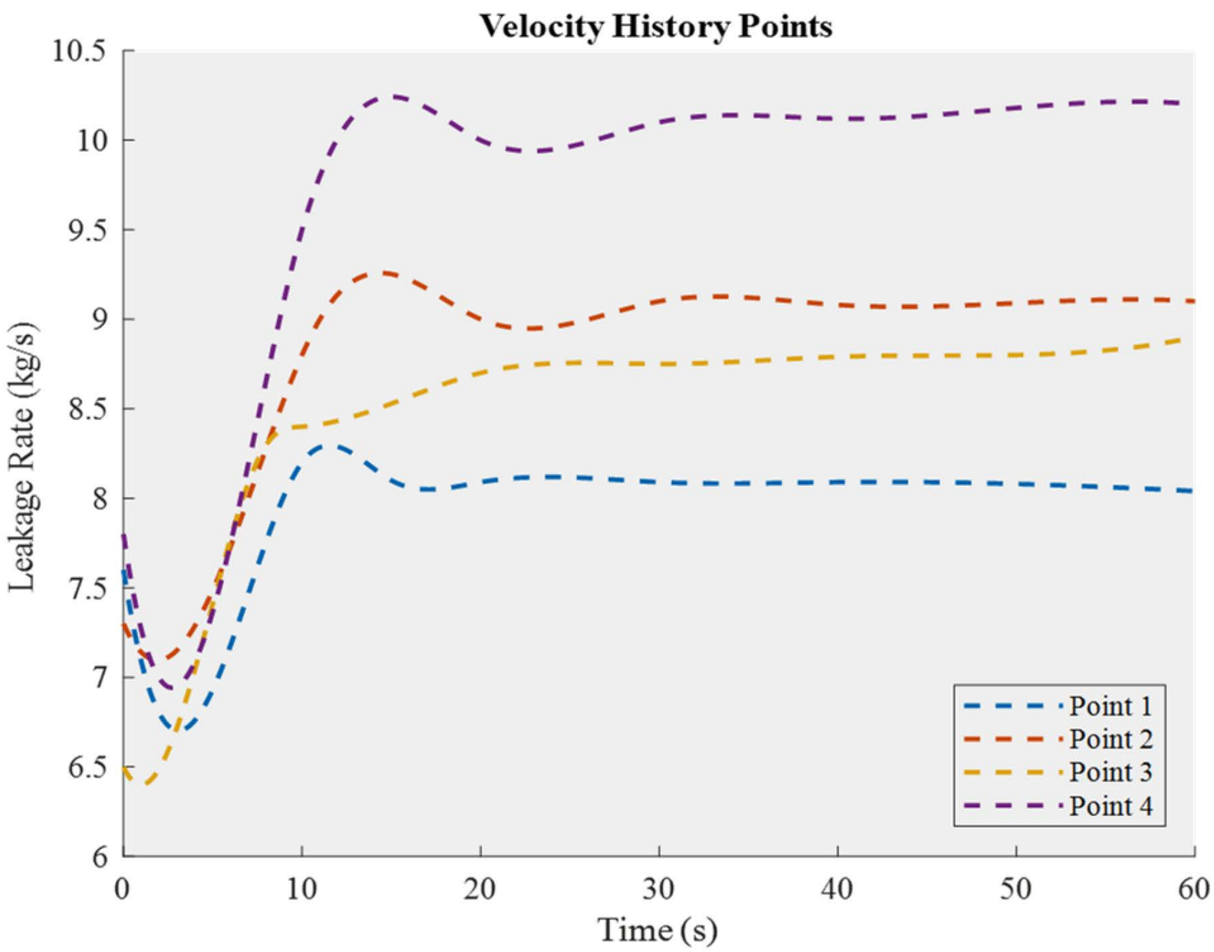

Figure 3. Leakage-rate variation at monitoring points.

From the perspective of mass and energy conservation, the release process of the medium inside the storage tank can be expressed as follows:

Mass balance relationship:

$$\frac{dM_{tank}}{dt} = -\dot{m}_{leak}$$

Energy balance relationship:

$$\frac{dU_{tank}}{dt} = -\dot{m}_{leak} \cdot h_{leak} + Q$$

M_{tank} is the mass of the medium inside the storage tank, U_{tank} is the internal energy of the storage tank, $\dot{m}_{leak}$ is the leakage mass flow rate, h_{leak} is the specific enthalpy of the leaking fluid, and Q is the heat exchange term between the environment and the storage tank. For short-term leakage processes, Q can be approximated as adiabatic or finite heat transfer according to the software model settings. The phase transition, temperature variation, and mass exchange during the leakage process jointly affect the CO_2 dispersion range and risk boundaries.

The KFX monitoring-point data indicate that the leakage rate after liquid CO_2 release did not monotonically decrease but instead exhibited a fluctuating pattern characterized by an initial decrease, subsequent increase, and gradual stabilization. This behavior is explained as follows: Significant thermodynamic phase transition behaviors occur during the leakage process of liquid CO_2. When high-pressure liquid CO_2 was released through a leakage orifice into a low-pressure environment, rapid depressurization caused liquid CO_2 to flash and absorb heat strongly, potentially reducing the temperature near the leak orifice to below −78.5 °C. Dry-ice particles then partially blocked the orifice, reducing the effective leakage area and lowering the leakage rate. Subsequently, continuous evaporation of liquid in the tank, heat input from the surroundings, and dry-ice sublimation reopened the leakage orifice, restored the pressure difference, and increased the leakage rate. In the later stage, as liquid CO_2 in the tank decreased, leakage of the remaining gaseous CO_2 was controlled by pressure equilibrium, and the leakage rate gradually stabilized as the tank and ambient pressures approached equilibrium. Around 20 s after leakage began, the leakage rates at the four monitoring points near the tank tended to converge, indicating that CO_2 dispersion had reached a quasi-steady state.

This process has direct significance for onsite response. If a temporary decrease in leakage rate during the early stage is interpreted as accident mitigation, the subsequent release risk after de-plugging may be underestimated. Therefore, temperature, pressure, and CO_2 concentration monitoring points should be arranged around the tank to identify ice-plugging and de-plugging through changes in leakage-orifice temperature, tank pressure, and near-field concentration. During emergency sealing, personnel should avoid approaching the leakage source blindly during temporary ice-plug formation. When necessary, remote isolation, shutdown, and depressurization should be implemented first, and the sealing window should then be selected according to temperature and pressure changes.

4. High-Concentration Risk Zoning and Emergency Management

4.1. Threshold System and Zoning Criteria

In this study, 3%, 5%, 7%, and 10% were used as safety monitoring and warning concentrations to identify general impact ranges and alarm-layout requirements, whereas 10%, 15%, 20%, and 30% were used as high-concentration acute-injury thresholds for risk zoning. The two threshold systems serve different purposes: the former emphasizes timely detection and alarm, whereas the latter emphasizes injury severity and emergency access control. This distinction avoids confusion between low-concentration monitoring boundaries and high-concentration injury boundaries.

The monitoring height from the CO_2 leakage point was set to 1.7 m. The maximum CO_2 dispersion ranges under the average temperatures of the coldest and hottest months were averaged to obtain mean maximum ranges. The maximum impact ranges for different concentrations of concern under different wind speeds and temperatures are listed in Table 6.

Based on the CO_2 concentration levels, human exposure effects, and emergency response requirements, the leakage area was classified into five risk zones: the fatality zone, severe injury zone, minor injury zone, adverse effect zone, and relatively safe zone. The outer envelope under unfavorable conditions should be preferentially adopted as the conservative control distance, while real-time wind direction, leakage duration, and the locations of off-site sensitive receptors should be used for dynamic adjustment. The final zoning results are shown in Table 7.

As shown in Table 7, after a CO_2 leakage accident, the area within 13 m downwind of the leakage point is the fatal zone, where the CO_2 concentration exceeds 300,000 ppm. Without protective measures, short-term exposure in this area can cause severe injury or death. Preventive measures must be taken immediately after leakage occurs. The injury-affected area extends from 13 to 33 m, where residents and personnel must be evacuated promptly and corresponding access-control measures must be implemented. Although areas beyond 33 m are relatively safe, exposure may still substantially increase respiratory demand and induce rapid breathing; therefore, a cordon should be established to prevent unauthorized personnel and residents from entering.

Table 6. Maximum impact range under different CO_2 concentrations of concern.

Wind Speed/(m·s^{-1})	Concentration Thresholds/ppm	Maximum Range/m (11.2 °C)	Maximum Range/m (24.5 °C)	Average Maximum Range/m
1.5	100,000	31.04	34.81	32.92
1.5	150,000	22.41	24.02	23.21
1.5	200,000	18.24	19.03	18.63
1.5	300,000	12.66	13.34	13.00
4.6	100,000	30.42	33.81	32.11
4.6	150,000	22.17	23.78	22.98
4.6	200,000	17.54	18.19	17.86
4.6	300,000	12.52	13.35	12.94
28	100,000	18.78	20.38	19.58
28	150,000	14.35	15.29	14.82
28	200,000	11.28	12.07	11.67
28	300,000	8.72	9.32	9.02

Table 7. Risk zoning results based on high-concentration CO_2 toxicity thresholds.

Wind Speed/(m·s^{-1})	Fatal Zone/m	Severe Injury Zone/m	Minor Injury Zone/m	Adverse Effect Zone/m	Relatively Safe Zone/m
1.5	<13	13–19	19–23	23–33	>33
4.6	<13	13–18	18–23	23–32	>32
28	<9	9–12	12–15	15–20	>20

4.2. Risk Quantification and Interpretation of Key Distances

The simplified calculation model based on the trapezoidal fuzzy relationship [36] was employed to describe the spatial distribution of leakage risk.

The risk index at the leakage source is defined as R_0 = 1, which represents the maximum risk level at the leakage source. Considering the attenuation characteristics of risk with increasing distance, a Gaussian spatial attenuation function was adopted:

$$R(x) = R_0 exp\left(-\frac{x^2}{2\sigma^2}\right)$$

$R(x)$: the relative risk index at a distance x from the leakage source;

R_0: the maximum risk index at the leakage source;

x: the distance from the leakage source;

σ: the risk diffusion scale parameter, representing the spatial attenuation range of the risk distribution.

This model reflects the gradual decrease in risk level with increasing distance after CO_2 leakage due to gas dispersion, dilution, and spatial transport processes. The risk index does not represent the probability of accident occurrence but rather serves as an auxiliary indicator to describe the relative variation of risk levels at different distances.

To account for the influence of exposure duration on CO_2 toxicity, the human exposure risk can be expressed as the combined effect of concentration and exposure time:

$$\text{Risk} = f(C,t)$$

C represents the CO_2 concentration, and t represents the exposure duration.

As the CO_2 concentration increases or the exposure duration becomes longer, the potential health risk to humans increases accordingly. Therefore, during emergency response, even if the instantaneous concentration in a specific area is below the high-concentration injury threshold, prolonged exposure may still result in significant exposure risks.

The calculated risk values for different areas near the leakage source are presented in Table 8.

Table 8. Risk values at different distances around the leakage source.

Distance from Leakage Point (m)	Risk Value
30	2.39×10^{-5}
50	2.03×10^{-5}
100	9.72×10^{-6}
120	5.49×10^{-6}
146	0

The original calculation results show that the risk values within 30 and 50 m of the leakage point are on the order of 10^{-5}, indicating areas requiring key prevention and access control. At 100 m from the leakage point, the risk value decreases to the order of 10^{-6}; however, leakage in this area may not be directly perceptible to personnel, and exposure risk may still occur in the absence of an alarm system. Therefore, CO_2 concentration monitoring and alarm systems are recommended within 100 m, and 146 m can be used as a reference for setting the maximum impact boundary and warning signs.

4.3. Monitoring, Alarm, and Emergency Evacuation Recommendations

Based on the dispersion simulations and risk zoning results, a layered control strategy of "near-source dense monitoring-downwind boundary alarm-off-site coordinated warning" should be established for oilfield CCUS ground injection systems. In near-source areas, high-density CO_2 concentration sensors should be deployed around CO_2 storage tanks, valve groups, flanges, and pipe racks, together with temperature and pressure monitoring. In intermediate-distance areas, alarm points should be arranged according to the prevailing wind direction and personnel activity routes. Continuous monitoring coverage should be provided within 100 m to ensure timely warning at low-perceptibility risk levels. The 146 m boundary may serve as an important reference for off-site warning signs and temporary cordon settings.

Emergency plans should define action requirements for each zone. Unprotected personnel should be prohibited from entering the fatal and severe-injury zones, and response actions should be performed by trained personnel wearing positive-pressure air-breathing apparatus. Personnel in the minor-injury and adverse-reaction zones should be evacuated immediately, and vehicles and unrelated personnel should be restricted. Cordon lines and upwind assembly points should also be established in relatively safe zones to prevent personnel from entering newly formed hazardous areas when wind direction changes. For adjacent residential areas, a coordinated response mechanism among the station alarm system, enterprise emergency team, local government, and village or community units should be established within 300 s.

5. Conclusions

(1) The PHAST-KFX two-stage simulation framework proposed in this study integrates the advantages of efficient multi-scenario accident screening and detailed three-dimensional dispersion analysis under complex site conditions. PHAST enables rapid identification of impact ranges under different leakage scenarios, while KFX further reveals the effects of buildings, equipment layouts, and near-ground boundaries on the dispersion pathways and local accumulation behavior of heavy CO_2 gas clouds. This approach overcomes the

limitations of conventional two-dimensional consequence models, which are unable to adequately characterize complex site-specific spatial effects, as well as the high computational cost associated with standalone CFD simulations. Therefore, the proposed framework provides an engineering-feasible approach for leakage risk assessment of oilfield CCUS ground facilities.

(2) The leak aperture is the dominant factor controlling the CO_2 leakage dispersion scale. When the leak aperture increased from 5 mm to 50 mm, the maximum dispersion distance increased from 8.8–9.4 m to 132–146 m, and the cloud footprint increased from 4.8–5.4 m^2 to 2204.1–2599.6 m^2, indicating that large-aperture leakage can cause significant outward expansion risk within a short time.

(3) Temperature and wind speed jointly affect the CO_2 concentration distribution. Higher temperature enhances dispersion capacity. Low wind speed tends to cause high-concentration near-field accumulation, whereas high wind speed may dilute near-field concentrations while enhancing long-distance downwind transport. Therefore, warning zones and evacuation routes should be dynamically adjusted according to real-time wind speed, wind direction, and meteorological conditions.

(4) Phase transition after CO_2 leakage can cause dry ice to block the leak orifice, resulting in repeated ice-plugging and de-plugging and a fluctuating leakage-rate pattern characterized by an initial decrease followed by an increase. This directly affects the timing of emergency sealing. Temperature and pressure sensors should therefore be installed around the tank to monitor leakage-orifice temperature and pressure changes in real time, predict ice-plugging risk, and determine the remaining CO_2 phase based on tank pressure. In the early stage of emergency response, dry ice should first be removed before rapid sealing is performed; later, ambient temperature should be controlled to prevent repeated ice-plugging.

(5) The accident-site environment is dynamically variable, and evacuation distances should be optimized according to actual conditions. The KFX simulation showed that CO_2 can generate airflow vortices among building clusters. Because these vortices have weak mixing with the ambient atmosphere, evacuation zones should be adjusted accordingly. When liquid CO_2 leakage occurs under sudden wind-direction changes, snowfall, or near-sunset conditions, the safe evacuation range should be expanded.

(6) Based on the CO_2 concentration thresholds and the effects of exposure duration, a risk zoning method was established by distinguishing between monitoring and alarm thresholds and acute injury risk thresholds. The results indicate that the area within 13 m downwind of the leakage point is the fatal zone, where short-term exposure can cause severe injury; the injury-affected area extends from 13 to 33 m, requiring timely evacuation and access control; areas beyond 33 m are relatively safe but can still increase respiratory demand by approximately ten times, so cordons should be established to prevent unauthorized access. Considering the risk-quantification results, CO_2 concentration monitoring and alarm systems are recommended within 100 m, warning signs should be placed at the maximum impact boundary of 146 m, and 300 s should be used as the control time window for plant evacuation and coordinated response with surrounding residential areas.

6. Limitations

(1) Future studies will further validate the numerical stability and reproducibility of the model results by incorporating mesh refinement analysis, time-step sensitivity analysis, and field monitoring data or controlled release experiments.

(2) Since some turbulence closure models and numerical implementation details within the commercial software PHAST and KFX are not fully disclosed, we did not perform

comparative analyses among different turbulence models. Future research can combine field monitoring data, controlled release experiments, or sensitivity analyses based on different turbulence closure models to further investigate the influence of turbulence model selection on CO_2 concentration distributions and risk zone boundaries.

(3) The sensitivity analysis in this study mainly focuses on three key engineering parameters: leakage aperture size, ambient temperature, and wind speed. Due to the large number of possible combinations involving different leakage orientations and building layout conditions, a global sensitivity analysis covering all parameter combinations was not performed. Future studies may employ orthogonal experimental design, machine learning surrogate models, or uncertainty quantification methods to further evaluate the effects of multi-factor interactions on risk boundaries.

(4) Since PHAST and KFX are commercial engineering software packages, some internal details of phase-change treatment and thermophysical property implementation are not fully disclosed. Future studies may combine detailed thermodynamic models, experimental data, or comparisons among different phase-change models to further investigate the effects of flashing, dry ice formation, and sublimation processes on leakage source terms and risk boundaries.

(5) The 300 s time window is dependent on the specific simulation conditions. The simulation results are based on a single site-specific layout and have not yet been generalized to other locations.

Author Contributions: Conceptualization, W.D.; Methodology, J.M.; Software, J.M.; Validation, W.D.; Formal Analysis, Y.B.; Resources, D.Z.; Data Curation, D.Z.; Writing—Original Draft, J.M.; Writing—Review and Editing, X.W. and A.Z.; Visualization, Y.Q.; Supervision, D.Z.; Project Administration, W.D. All authors have read and agreed to the published version of the manuscript.

Funding: This research was funded by the Shandong Provincial Science and Technology SMEs Innovation Capacity Improvement Project (Grant No. 2025TSGCCZZB0278) and the Qingdao West Coast New Area Science and Technology Project (Grant No. 2024-21).

Data Availability Statement: Data are included within the submitted manuscript; further inquiries can be directed to the corresponding author.

Conflicts of Interest: Authors Xiaoyu Wang, Yue Qi and Yanbin Bi were employed by the PetroChina Liaohe Oilfield Company. The remaining authors declare that the research was conducted in the absence of any commercial or financial relationships that could be construed as a potential conflict of interest.

References

1. Bi, L.; Li, J.; Zhang, Y.; Min, L.; Yan, R.; Zhan, L.; Yang, N.; Yang, S.; Chen, Z. Pore-scale numerical modeling of transport kinetics for CCUS-EOR and carbon cycling in offshore–onshore integrated energy system. *Fuel* **2026**, *403*, 136122. [CrossRef]
2. Tardin-Coelho, R.; Bharadwaj, B.; Ashworth, P. Carbon capture utilisation and storage (CCUS) and public perceptions: A systematic literature review. *Int. J. Greenh. Gas. Control* **2025**, *145*, 104393. [CrossRef]
3. Su, X.; Liu, P.; Mei, Y.; Qiu, J. The impact of carbon capture, utilization, and storage (CCUS) projects on environmental protection, economic development, and social equity. *J. Clean. Prod.* **2024**, *482*, 144218. [CrossRef]
4. IPCC. *Global Warming of 1.5 °C. An IPCC Special Report on the Impacts of Global Warming of 1.5 °C Above Pre-Industrial Levels and Related Global Greenhouse Gas Emission Pathways, in the Context of Strengthening the Global Response to the Threat of Climate Change, Sustainable Development, and Efforts to Eradicate Poverty*; World Meteorological Organization: Geneva, Switzerland, 2018.
5. Kang, N.; Sarsenbekuly, B.; Wu, H. Progress of CCUS technology with enhanced oil recovery. *J. CO_2 Util.* **2025**, *102*, 103233. [CrossRef]
6. IEA. *CCUS Projects Database*; International Energy Agency: Paris, France, 2023.
7. Xu, D. Reflections on the recent oil spill from a pipeline in the United States. *China Pet. Petrochem.* **2023**, *34*.
8. Shang, Y.; Chen, X.; Yang, M.; Xing, X.; Jiao, J.; An, G.; Li, X.; Xiong, X. Comprehensive review on leakage characteristics and diffusion laws of carbon dioxide pipelines. *Energy Fuels* **2024**, *38*, 10456–10493. [CrossRef]

9. Sori, A.; Moghaddas, J.; Abedpour, H. Comprehensive review of experimental studies, numerical modeling, leakage risk assessment, monitoring, and control in geological storage of carbon dioxide: Implications for effective CO_2 deployment strategies. *Greenh. Gas. Sci. Technol.* **2024**, *14*, 887–913. [CrossRef]
10. Li, X.; Liu, T.; Zhang, L.; Zhou, H.; Liu, G.; Wang, Y.; Gan, M.; Li, Q. Carbon sequestration technology: Challenges and urgent critical scientific issues. *Coal Geol. Explor.* **2026**, *54*, 3. [CrossRef]
11. Li, C.; Marquez, J.A.D.; Hu, P.; Wang, Q. CO_2 pipelines release and dispersion: A review. *J. Loss Prev. Process Ind.* **2023**, *85*, 105177. [CrossRef]
12. Tan, J.; Xin, Y.; Liu, W.; Jing, Y.; Hu, H. Progress on the leakage and diffusion characteristics of CO_2 pipelines. *Fuel* **2026**, *425*, 139474. [CrossRef]
13. Yang, X.; Qiao, F.; Yan, X.; Yu, S.; Liu, Z.; He, Y.; Yu, J. Experimental study on leakage and diffusion risks of impurity-containing dense-phase CO_2 pipelines at industrial scale. *Process Saf. Environ. Prot.* **2026**, *207*, 108409. [CrossRef]
14. Yang, H.; Yang, Y.F.; Zhang, Q.; Duan, Q.; Liu, X.; Ouyang, X. Research on quantitative risk assessment of repurposing in-service oil and gas pipelines for CO_2 transport. *Pipeline Prot.* **2025**, *2*, 19–31. [CrossRef]
15. Hu, Q.; Zhang, H.; Zhao, X.; Meng, L.; Li, Y.; Zhang, L.; Zhu, J.; Wang, W. Carbon dioxide pipeline leakage risk assessment based on pipeline failure probability correction and CO_2 concentration dispersion distance prediction. *J. Pipeline Sci. Eng.* **2025**, *6*, 100293. [CrossRef]
16. Zhang, H.; Wang, S.; Jia, X.; Wang, F. Risk Level Assessment and Impact Range Analysis of CCUS CO_2 Pipeline Leakage Based on Machine Learning. *Safety* **2026**, *12*, 44. [CrossRef]
17. Chen, B.; Harp, D.R.; Zhang, Y.; Oldenburg, C.M.; Pawar, R.J. Dynamic Risk Assessment for Geologic CO_2 Sequestration. *arXiv* **2021**, arXiv:2109.12703.
18. Saini, P.; Biradar, U.; Sonawane, K. A hybrid monitoring framework for identifying leaks in CCUS pipelines using computer vision and sensor fusion. In *Proceedings of the 26th International Conference on CCUS & Environmental Excellence (26 JCUS)*; SPE: Richardson, TX, USA, 2026; Volume 26, p. D021S012R001.
19. Al-Yaari, A.; Ching, D.L.C.; Sakidin, H.; Muthuvaiu, M.S.; Zafar, M.; Haruna, A.; Merican, Z.M.A.; Yunus, R.B.; Al-dhawi, B.N.S.; Jagaba, A.H. The effects of nanofluid thermophysical properties on enhanced oil recovery in a heterogeneous porous media. *Case Stud. Chem. Environ. Eng.* **2024**, *9*, 100556. [CrossRef]
20. Chen, B. Quantitative simulation analysis of CO_2 pipeline leakage and diffusion based on PHAST software. *Energy Conserv. Meas. Pet. Petrochem. Ind.* **2024**, *14*, 63–68.
21. Di Franco, F.; Russo, D.; Di Benedetto, A. Comparative risk analysis of aqueous formate solutions and compressed hydrogen storage: Safety and scalability assessment. *Int. J. Hydrogen Energy* **2026**, *230*, 154773. [CrossRef]
22. Portarapillo, M.; Di Benedetto, A. Design and risk assessment of integrated H2 fuel cell systems for rail transportation. *Int. J. Hydrogen Energy* **2026**, *223*, 154382. [CrossRef]
23. Bhardwaj, S.; Bajaj, C. PHAST: Port-Hamiltonian Architecture for Structured Temporal Dynamics Forecasting. *arXiv* **2026**, arXiv:2602.17998.
24. Sarebanzadeh, K. Dispersion of LPG from spherical storage tanks: Power-law scaling and comparative analysis of LFL vs. 50% LFL. *PLoS ONE* **2026**, *21*, e0341322. [CrossRef] [PubMed]
25. Shin, D.W.; Choi, Y.; Lee, K.; Choi, S.J.; Moon, S.M.; Kim, E.S.; Kim, H.B.; Park, J.S.; Song, K.H. P-1996. Performance Evaluation of an Artificial-Intelligence-Driven Single-Cell Imaging Platform for Rapid Phenotypic Antimicrobial Susceptibility Testing. *Open Forum Infect. Dis.* **2026**, *13*, ofaf695.2161. [CrossRef]
26. Vianello, C.; Macchietto, S.; Maschio, G. Conceptual Models for CO_2 Release and Risk Assessment: A Review. *Chem. Eng.* **2012**, *26*, 573–578.
27. Witlox, H.W.M.; Harper, M.; Oke, A.; Stene, J. Phast validation of discharge and atmospheric dispersion for pressurised carbon dioxide releases. *J. Loss Prev. Process Ind.* **2014**, *30*, 243–255. [CrossRef]
28. Hsieh, L.F. Dense gas dispersion modelling of CO_2 released from carbon capture and storage infrastructure into complex environment. *Int. J. Green-House Gas. Control* **2013**, *17*, 127–139. [CrossRef]
29. Jang, C.B.; Choi, S.; Baek, J. CFD modeling and fire damage analysis of jet fire on hydrogen pipeline in a pipe rack structure. *Int. J. Hydrogen Energy* **2015**, *40*, 15760–15772. [CrossRef]
30. Nubli, H.; Sohn, J.M. CFD-based analysis of an accidental jet-fire release on LNG bunkering vessel. In *Proceedings of 7th International Conference on Industrial, Mechanical, Electrical and Chemical Engineering 2021 (ICIMECE 2021)*; AIP Publishing LLC: Melville, NY, USA, 2023; Volume 2674, p. 030040. [CrossRef]
31. Rian, K.E. Modelling and numerical simulation of hydrogen jet fires for industrial safety analyses–Comparison with large-scale experiments. In Proceedings of the 8th International Conference on Hydrogen Safety (ICHS 2019), Adelaide, Australia, 24–26 September 2019.
32. Kumaresh, G.R.; Fossan, I.; Venkatraman, M.M.; Giljarhus, K.E.; Spangelo, Ø.; Jensen, S. CFD-based transient ignition probability modeling of gas leaks in enclosures. *Int. J. Comput. Methods* **2016**, *13*, 1640006. [CrossRef]

33. Kim, C.; Choi, B.C. Dispersion analysis of the unignited flare gas in an LNG-FPSO vessel. *J. Adv. Mar. Eng. Technol. (JAMET)* **2017**, *41*, 753–759. [CrossRef]
34. *GB/T 37243-2019*; Determination Method of External Safety Distance for Hazardous Chemicals Production Units and Storage Installations. Standards Press of China: Beijing, China, 2019.
35. *GBZ 2.1-2019*; Occupational Exposure Limits for Hazardous Agents in the Workplace—Part 1: Chemical Hazardous Agents. China Standards Press: Beijing, China, 2019.
36. Jia, B.; Le, P.; Kang, X.; Lei, X.; Zhou, M. Leakage risk evaluation model for wells in the process of CO_2 storage in low permeability reservoirs. *Front. Earth Sci.* **2019**, *9*, 112.

https://doi.org/10.3390/pr14152383